THE JOURNAL OF PHYSICAL CHEMISTRY C

Article

pubs.acs.org/JPCC

Facile and Green Preparation for the Formation of MoO_2-GO Composites as Anode Material for Lithium-Ion Batteries

Shan Hu,[†,‡] Fei Yin,[†] Evan Uchaker,[‡] Wen Chen,*[,†] Ming Zhang,[‡] Jing Zhou,[†] Yanyuan Qi,[†] and Guozhong Cao*[,‡]

[†]State Key Laboratory of Advanced Technology for Materials Synthesis and Processing, School of Materials Science and Engineering, Wuhan University of Technology, Wuhan, 430070, P. R. China

[‡]Department of Materials Science and Engineering, University of Washington, Seattle, Washington 98195, United States

Supporting Information

ABSTRACT: A facile and green hydrothermal method has been developed to fabricate three-dimensional nanoarchitecture composites consisting of MoO_2 nanoparticles decorated on the graphene oxide (GO). The composites were characterized by XRD, SEM, and HRTEM. It was demonstrated that MoO_2 nanoparticles are 5−15 nm in size and homogeneously dispersed on GO and denoted as MoO_2-GO composites. When tested as an anode material for lithium-ion batteries, the MoO_2-GO composites exhibited an improved storage capacity and cycling performance, higher than the pure MoO_2 nanoparticles. As a result, the GO effectively forms a conductive network that greatly enhances the electrical conductivity and structural stability of composites. The incorporation of the flexible and conductive GO and the small homogeneous MoO_2 nanoparticles could not only maintain the structural and electrical integrity, but also accommodate the volume change during the lithium-ion intercalation and de-intercalation. The ultrafine MoO_2 nanoparticles dispersed on the GO are beneficial to the improved electrochemical performance of the composites, which makes them a promising anode candidate for lithium-ion batteries.

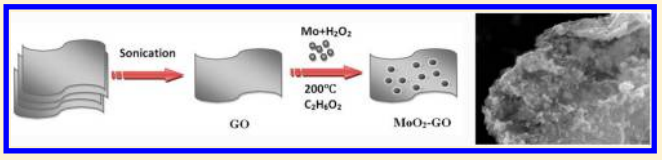

1. INTRODUCTION

With the fast-growing demand on petroleum resources and gaseous emissions from the burning of fossil fuels, the use of traditional fuel sources will not only bring about the increasing scarcity of petroleum, but also create environmental deterioration such as global warming with alarming consequences.[1−3] In order to alleviate the dependence on petroleum and decrease CO_2 emissions, it is particularly crucial to develop new and renewable energy resources. With their high energy/power density, long cycling life, and environmental benignity, lithium-ion batteries (LIBs) have been regarded as one of the most promising candidates for the power sources of electric vehicles and mobile electronics worldwide.[4−6] To meet the continuously urgent demand in large-scale energy applications such as electric vehicles, renewable power plants, and electric grids, substantial works have been dedicated to exploiting novel structural and competitive energy storage materials with high power density and safety performance.[7−9]

In order to achieve the high power density and rapid ionic and electronic diffusion in electrode materials, many strategies have been developed to enhance the electrochemical performance.[10] In recent years, many studies have focused on tailoring materials to the nanoscale, the characteristics of which include large specific surface area and confined material dimension that allow the material to achieve a high lithium-ion intercalation capability. In addition, better electrochemical performance can be realized because of the fast charge transfer kinetics and enhanced lithium-ion diffusion in the nanomaterial storage system. It has also been revealed that nanomaterials can provide a shortened transport path for electrons and lithium ions, which is beneficial for the discharge/charge processes under the large currents.[11−13] Moreover, nanomaterials can accommodate large volume expansion during intercalation, resulting in improved lifespan with better cyclic stability. Additionally, the large contact area between nanomaterials of the electrode and the electrolyte not only reinforces the intercalation activity of the lithium-ion, but also leads to higher discharge/charge rates. Because of the short transportation path and large specific surface area, the nanostructured transition metal oxides were highly used as the electrode of LIBs, which can obtain an improved capability of storage lithium-ions. Among them, MoO_2 has attracted significant attention as a potential electrode material, due to its high theoretical capacity (838 mA h g^{-1}), high thermal stability, low metallic electrical resistivity, and affordable cost.[14−16]

The monoclinic structure of MoO_2 can be viewed as a distorted version of the rutile crystal structure (as shown in Figure 1).[17−19] The Li-ion is inserted in the octahedral interstitial sites, in the "tunnels" between the chains, to form Li_xMoO_2, which was first reported as a host material 30 years ago.[17,18,20,21] A high theoretical capacity can be obtained when four lithium-ions are incorporated per each MoO_2 formula

Received: September 4, 2014
Revised: September 30, 2014
Published: October 2, 2014

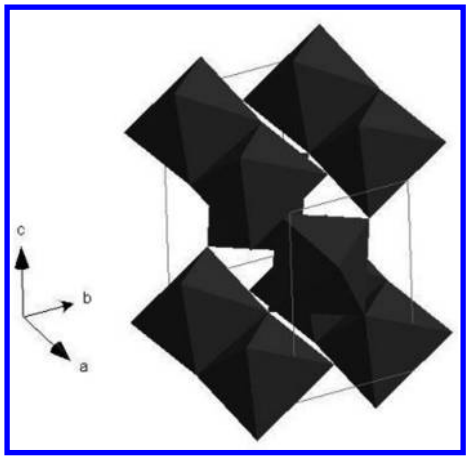

Figure 1. Structure diagram of monoclinic MoO_2.

unit.[22] Unfortunately, this high degree of lithium-ion incorporations makes it difficult for MoO_2 to adjust to the structural expansion resulting from the phase transformation during the charging/discharging process. At the same time, large volume expansions occur during the lithium-ion intercalation/de-intercalation process, leading to plugging of the electrical contact pathways as well as the active material breaking away from the current collector and resulting in severe fading of the capacity and poor cycling stability.[18,23] One effective way to alleviate this problem is to design and fabricate the nanostructure to improve the electrochemical performance of electrode materials by shortening the diffusion pathways for electrons and lithium-ions, increasing the contact surface areas between the electrode material and electrolyte, and enhancing the reaction activity.[24,25] It has been confirmed by many researchers that nanostructured MoO_2 has improved electrochemical properties when assembled as lithium-ion battery anodes compared to their bulk counterparts.[26,27] Wang et al.'s report revealed the ability of carbon-coated MoO_2 nanospheres to deliver a reversible capacity of 570 mA h g^{-1} after 30 cycles.[28] Xu et al. modified MoO_2 nanopaticles with graphite oxide to achieve a high, reversible capacity of 720 mA h g^{-1} at a current density of 100 mA g^{-1}.[29] Liu et al. demonstrated that MoO_2 nanostructured particles can be easily obtained by a facile and template-free one-pot strategy. In addition, MoO_2 nanoparticles used as anode materials for LIBs have a high specific capacity of 824 mA h g^{-1} at C/10 and high reversible capacity of 760 mA h g^{-1} after 30 cycles.[24] Another effective way is to fabricate a conductive hybrid through the combination of molybdenum dioxide and carbonaceous matrix materials to improve the structural integrity and accommodate great volume variation during the lithium-ion insertion/extraction process, hence the cycling performance.[30−32] Zhou et al. fabricated carbon-coated MoO_2 nanocrystals with a facile hydrothermal process, which exhibited high specific capacities of 640 mA h g^{-1} at and 575 mA h g^{-1} at 200 mA g^{-1} and 400 mA g^{-1}, respectively, and improved cycling stability.[33] Zeng et al. reported that the nanocomposite of MoO_2-ordered mesoporous carbon can obtain a reversible capacity up to 689 mA h g^{-1} after 50 cycles when cycled at a current density of 50 mA g^{-1}. It can attain a high reversible capacity of 401 mA h g^{-1} at a current density as high as 2 A g^{-1}.[23] Seng et al. reported that the facile synthesis process of graphene-MoO_2 composites with the highest MoO_2 ratio can deliver a higher reversible capacity and excellent cycling stability at low rates.[34] Sun et al.'s work demonstrated that a hierarchical graphene-MoO_2 structure can retain good cycling stability for up to 70 cycles.[26] Evidently, previous researchers have indicated that the composite structure based on MoO_2 and carbonaceous matrix materials, especially graphene nanosheets, is highly promising as high-performance anode electrodes for LIBs.[27,28,35] As far as we know, many studies focus on the synthesis of graphene/MoO_2 composites; there are few reports about synthesis of MoO_2 nanoparticles embedded on GO employing a facile and environmentally friendly route. It is important to construct a novel nanoarchitecture that combines the advantages of accessible strategy and graphene oxide to make better use of their dramatic properties in potential electrode materials. Therefore, both the improved discharge capacity and cycling performance of MoO_2 based anode electrode materials are strongly desirable for the design of high performance LIBs.

In this study, we report a facile and green hydrothermal method to directly obtain MoO_2-GO composites following by the addition of ethylene glycol to form a conductive three-dimensional nanoarchitecture. Ethylene glycol, a cheap and common solvent, acted as a reducing and surfactant agent, which aided in the formation of MoO_2 nanoparticles. Furthermore, electrochemical tests revealed that the as-prepared MoO_2-GO composites exhibited enhanced lithium-ion storage capacity and better cycling stability as anode materials for LIBs when compared with the pure MoO_2 nanoparticles.

2. EXPERIMENTAL METHODS

2.1. Material Synthesis. Graphene oxide (GO) was prepared using graphite powder (Aldrich, powder, <20 μm, synthetic) according to a modified Hummers method.[36] Exfoliation was carried out by sonicating the GO dispersion (4 mg mL^{-1}) under ambient conditions.[37] The MoO_2-GO composite was synthesized via a hydrothermal route. All chemicals used in this study were analytical grade and used as received without purification. In a typical synthesis, 12 mmol of commercial molybdenum powder was placed in a wide-mouth bottle, and 29 mmol of hydrogen peroxide was added gradually under stirring. GO mixed with ethylene glycol was added into the solution, followed by stirring and sonication at room temperature for 3 h. Then, the mixture was sealed in a PTFE-lined stainless steel autoclave and kept at 200 °C for 24 h to obtain MoO_2-GO composites. When the autoclave cooled down to room temperature, the resulting precipitate was washed with deionized water repeatedly, then collected by centrifugation, following by drying precipitate at 80 °C. The formation of the product is shown in Scheme 1. For comparison purposes, the pure MoO_2 nanoparticles were also prepared for the electrochemical test in the same environment.

2.2. Materials Characterization. X-ray diffraction (XRD, D8 Bruker X-ray diffractometer) was carried out to analyze the crystal structure of the as-prepared sample, which was scanned

Scheme 1. Schematic Depicting the Formation of MoO_2-GO Composites

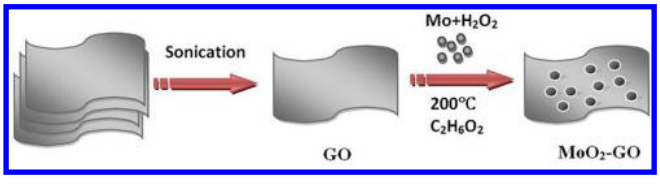

dx.doi.org/10.1021/jp508933c | J. Phys. Chem. C 2014, 118, 24890−24897

with Cu Kα radiation (λ = 1.5418 Å). Scanning electron microscopy (SEM, JEOL, JSM-7000F) and transmission electron microscopy (TEM, FEI, Tecnai G2 F20) were used to examine the morphology and microstructure of the as-prepared samples.

2.3. Electrochemical Measurement. The working electrode was prepared by a slurry coating procedure.[38] The slurry was composed of active material, carbon black, and polyvinylidene fluoride (PVDF) dispersed in *N*-methylpyrrolidinone (NMP) in the weight ratio of 80:10:10. The slurry was uniformly spread and pasted onto a piece of Al foil as the working electrode. Then, the as-prepared mixture was dried in a vacuum oven at 80 °C for 6 h before assembling the coin cell. CR2016-type coin cells were assembled in a glovebox (Innovative Technology, IL-2GB), which was filled with pure Ar gas with the lithium foil as the counter electrodes, and polypropylene film as the separate. 1 M $LiPF_6$ solution in a volume ratio of 1:1 mixture of ethylene carbon (EC)/dimethyl carbonate (DMC) was used as the electrolyte. Finally, the assembled coin cells were aged at room temperature overnight before the electrochemical test.

Cyclic voltammetry (CV) was conducted by using an Arbin electrochemical workstation (Arbin Instruments, College Station) at a scan rate of 0.2 mV s^{-1} in the voltage range between 3 and 0.01 V. The assembled coin cells were galvanostatically discharged and charged under various current densities in the voltage range of 3.0−0.01 V (vs Li/Li^+). Alternating current (AC) impedance was carried out on a Solatron 1260 impedance analyzer in the frequency range ~0.01 Hz to 100 kHz.

3. RESULTS AND DISCUSSION

XRD was first employed in order to gather information on the crystallinity and phase of the as-prepared product. Figure 2 demonstrates the XRD patterns of MoO_2 nanoparticles and MoO_2-GO composites. All the diffraction peaks of both samples could be assigned to the pure monoclinic MoO_2 phase. The lattice parameters (a = 5.660 Å, b = 4.860 Å, c = 5.645 Å and β = 120.94°) were consistent with the values in the reports (JCPDS: 00−078−1073). No characteristic peaks are observed for impurities such as phosphates or MoO_3, as well as other molybdenum oxides. It is shown that no obvious differences exist between the two XRD patterns. However, the intensity of MoO_2-GO composites is slightly lower than that of MoO_2 nanoparticles due to the presence of GO, which is in good agreement with the previous report.[26,39] No significant sharpening of the diffraction peaks is observed after adding the graphene oxides, which suggests that crystal growth has been effectively suppressed by the formation of a graphene oxide network surrounding the nanocrystal.[40] In addition, all the diffraction peaks are strong and narrow, and the noise peaks decrease after introducing graphene oxides, which attests to the high crystallinity of the as-synthesized MoO_2-GO composites.

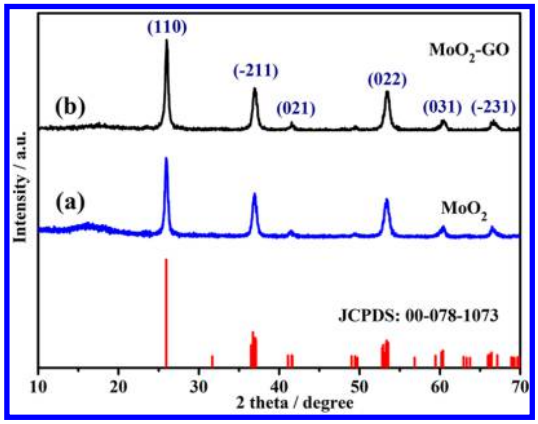

Figure 2. XRD patterns of (a) MoO_2 nanoparticles and (b) MoO_2-GO composites.

Scanning electron microscopy (SEM) and transmission electron microscopy (TEM) were carried out to investigate the microstructure and morphology of the as-synthesized samples. As shown in Figure 3a, at low magnification, it is found that the composite consists of aggregate nanoparticles to form the network structure. Figure 3b displays a magnified image, showing that the composites are composed of curled nanosheets and disorderly nanoparticles. It reveals a loose decoration of MoO_2 nanoparticles on graphene oxide nanosheets. The diameter of the nanoparticles is estimated to be 15 nm which is much smaller than that of MoO_2 previously reported.[29] MoO_2 nanoparticles (bright spot) are spreading over the flexible graphene oxide nanosheets, which can be distinguished as linear strips. A few MoO_2 nanoparticle aggregations are observed. The composites are composed of graphene oxide nanosheets and MoO_2 nanoparticles, which look like points of light to bedeck the evening sky (as shown in Figure 3c). This unique structure is believed to be three-dimensionally interconnected, which is favorable for enhancing the electrochemical properties for the storage of lithium-ions. In addition, the absence of charging during FESEM characterization implies that the nanocomposites are highly conductive due to the three-dimensional interconnection between particles. Figure 4a and b shows typical TEM images of the MoO_2-GO composites, where the MoO_2 nanocrystals, with size ranging from 5 to 15 nm, are embedded in the thin GO sheets. It looks like a crumpled piece of thin fabric with lots of folding on the edge. It is clearly seen that discrete MoO_2 nanoparticles are dispersed on GO even after sonicattion process for TEM observation. In addition, the nanocrystals are tightly coated on the GO which indicates that there is a strong connection from

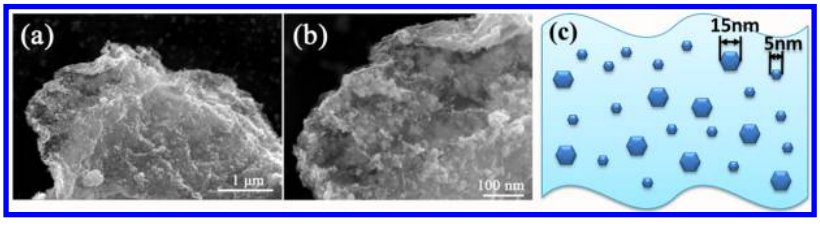

Figure 3. (a,b) SEM images of the resulting MoO_2-GO composites obtained by hydrothermal method. (c) Simplistic schematic diagram of the MoO_2-GO composites.

dx.doi.org/10.1021/jp508933c | J. Phys. Chem. C 2014, 118, 24890−24897

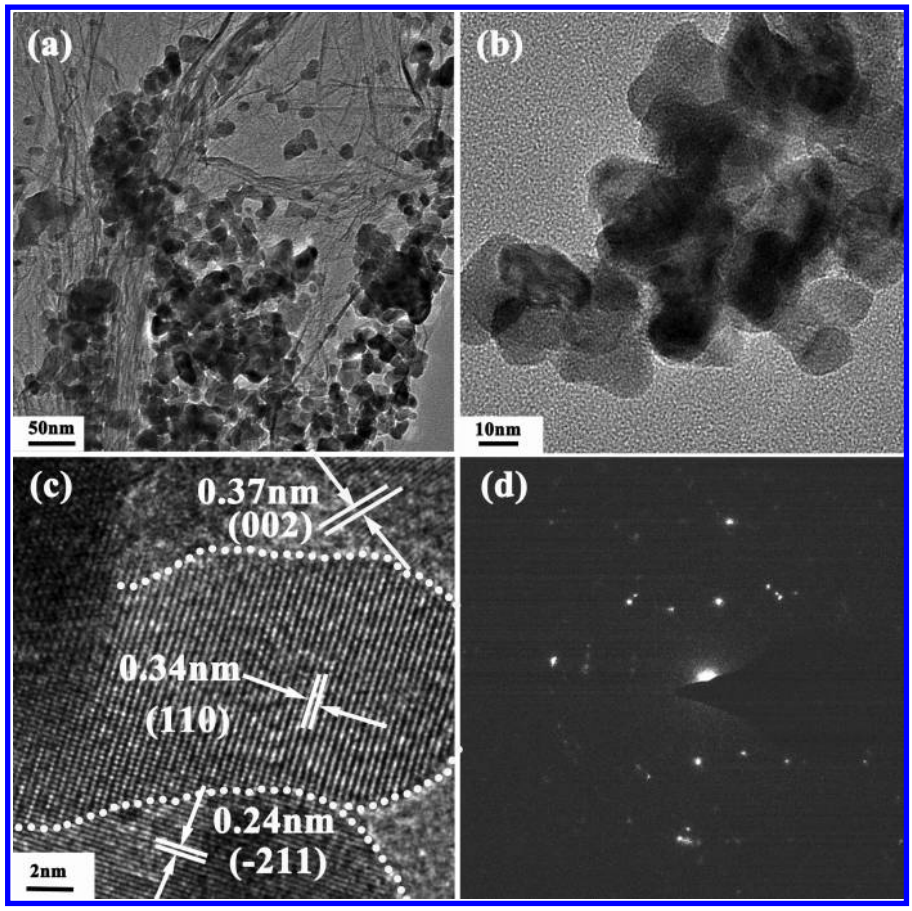

Figure 4. (a) (b) TEM images; (c) HRTEM image; (d) SAED pattern of the MoO_2-GO composites.

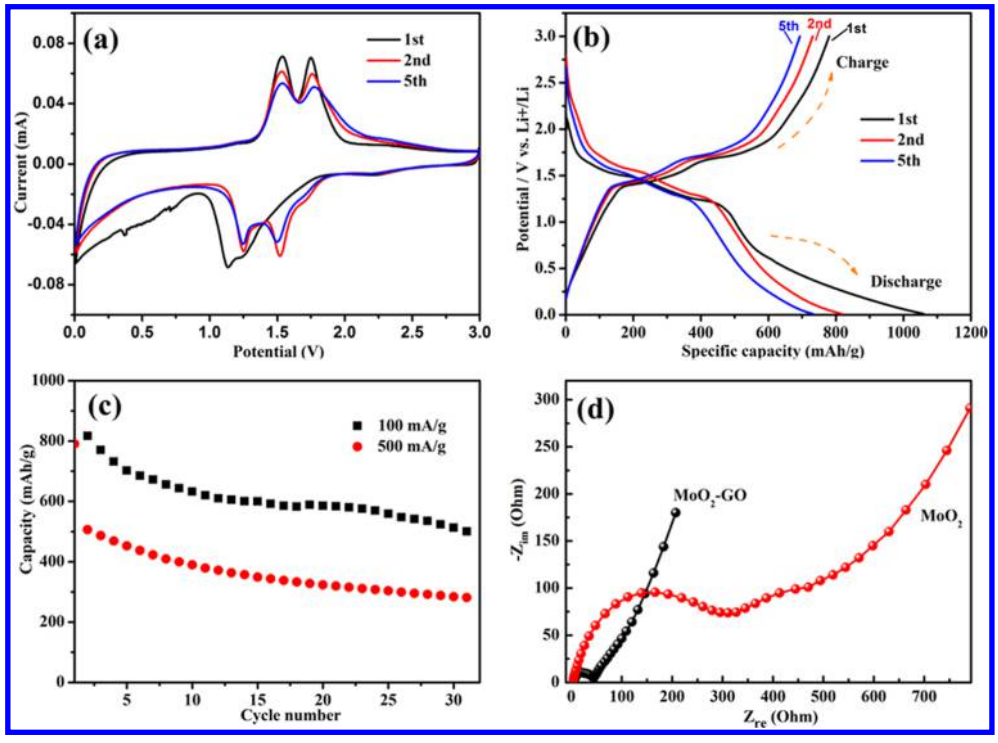

Figure 5. (a) Cyclic voltammograms of MoO_2-GO composites at 0.2 mV s^{-1}. (b) Charge/discharge profiles of MoO_2-GO composites at a current density of 100 mA g^{-1}. (c) Cycling performance of MoO_2-GO composites at current densities of 100 and 500 mA g^{-1}. (d) Nyquist plots of MoO_2-GO composites and the pure MoO_2 nanoparticles.

dx.doi.org/10.1021/jp508933c | J. Phys. Chem. C 2014, 118, 24890−24897

the MoO_2 nanoparticles to the GO nanosheets. TEM observation confirmed that the microstructure and morphology of the composites match well with those of the SEM observation. As shown in Figure 4d, the diffraction ring pattern obtained from selected area electron diffraction (SAED) can be assigned to the monoclinic MoO_2, indicating the polycrystalline nature of the sample. Two nanoparticles, which are marked by dotted lines, provide more detailed structural information as seen in Figure 4c. From the HRTEM image the lattice fringes of the MoO_2 nanoparticles can be clearly observed, suggesting the presence of a well-defined crystal structure. The periodic lattice fringe spaces were found to be 0.34 and 0.24 nm shown in Figure 4c corresponding to the interplanar spacings of the (110) and the (−211) planes, respectively, for monoclinic MoO_2 (JCPDS: 00−078−1073); these results further corroborate the findings from XRD. In addition, a nanolayer of several nanometers exists on the surface of the MoO_2 nanocrystals (Figure 4c). The 0.37 nm of interplanar spacing marked by a white frame is in good agreement with the (002) lattice plane of graphene oxide, which is much larger than that in the pristine graphite (0.34 nm). This supports the claim that the MoO_2 nanoparticle assemblies are well wrapped in the nanocarbon layer of graphene oxide nanosheets.

Next, the electrochemical properties of the as-obtained MoO_2-GO composites were evaluated. Figure 5a demonstrates that cyclic voltammetry (CV) curves were performed at a scan rate of 0.2 mV s^{-1} between 3.0 and 0.01 V at room temperature. During the first five cycles, obviously, the peak position is not substantially the same. In the first cycle, there are two reduction peaks at 1.18/1.25 V and two pronounced oxidation peaks at 1.51/1.75 V appeared, corresponding to the plateaus at the charge and discharge curves, respectively. The reduction peak at 1.18/1.25 V could be attributed to two steps of phase transition: from the monoclinic to the orthorhombic phase transition and orthorhombic to the monoclinic phase during Li-ion intercalation process, which was reported by Sun and Dahn.[26,41] It can be seen that two oxidation peaks observed at 1.51/1.75 V are ascribed to the phase transitions during the lithium-ion deinsertion. It is worth noting that, in the first cathodic sweep, a broad irreversible peak appeared at ∼0.7 V but disappeared during the following cycles, which is responsible for the formation of a solid electrolyte interface (SEI) film. The appearance of SEI film peak in the first cycle is consistent with the report of Yang et al. and Han et al.[27,39] This broad peak may lead to irreversible reaction in the first cycle, which brings about decay of the Coulombic efficiency and loss in the discharge capacity.[42] In the subsequent cycles, two evident redox peaks were observed at about 1.51/1.26 V and 1.52/1.74 V, which could be assigned to the reversible phase transitions of partially lithiated Li_xMoO_2 during lithium-ion insertion and extraction. Even after 5 cycles, the two pronounced redox couples still exist, which can be responsible for the highly reversible phase transformations. The CV profiles of the redox peaks remain almost the same during cycling which implies that the good stability and reversibility of the as-synthesized MoO_2-GO composites for lithium-ion insertion and extraction. The intensities of these two redox peaks gradually decrease during the subsequent cycles, which is probably because Li_xMoO_2 would convert to Mo and Li_2O when the potential drops below 1.0 V.[43] The good reversibility of the MoO_2-GO composites for lithium-ion insertion and extraction is dependent on the smaller MoO_2 particle size and the incorporation with GO.

Figure 5b shows a charge and discharge profile of the MoO_2-GO composite electrode at a current rate of 100 mA g^{-1} in the potential range of 0.01−3.0 V. The initial discharge and charge capacity is about 1060.1 and 779.9 mA h g^{-1}, respectively, with a Coulombic efficiency of 73.6%. The capacity loss (26.4%) of the initial cycle may be mainly attributed to the irreversible reduction of MoO_2 to Mo, the decomposition of electrolyte, and the formation of a solid electrolyte interface (SEI), which are common for most anode materials.[44−46] In fifth cycle, the Coulombic efficiency of the anode sample reaches 95.1%, which indicates good lithium-ion insertion/extraction performance during the cycling process. In the first cycle, there are two discharge and charge voltage plateaus appearing at 1.55/1.25 V and 1.47/1.73 V, which is in good agreement with the CV results. The above results could be ascribed to the phase transitions in the partially lithiated Li_xMoO_2. During the subsequent cycles, the plateaus become smooth, which is very common in the MoO_2 based anode materials. In the first cycle, the formation of Li_xMoO_2 could be explained for the Li-ion insertion into the structure of MoO_2, which is presented as eq 1. During the discharge and charge process, Li_xMoO_2 could resolve gradually into Li_2O and Mo, resulting in the gradual appearance of the phase transformation plateaus of Li_xMoO_2 (eq 2).[25,43] These results are consistent with the CV profiles, which show that the intensity of the insertion/deinsertion peaks decreases during these cycles.

$$x\mathrm{Li}^+ + x\mathrm{e}^- + \mathrm{MoO_2} \leftrightarrow \mathrm{Li}_x\mathrm{MoO_2} \qquad (0 < x < 0.98) \tag{1}$$

$$\mathrm{Li}_{0.98}\mathrm{MoO_2} + 3.02\mathrm{Li} \leftrightarrow 2\mathrm{Li_2O} + \mathrm{Mo} \tag{2}$$

In order to evaluate the cycling stability of the MoO_2-GO composites, the cycling performances of the as-prepared anode materials at 100 and 500 mA g^{-1} are demonstrated in Figure 5c. A discharge capacity of as high as 817.6 mA h g^{-1} is achieved when cycled at 100 mA g^{-1} in the first cycle. There is a slight decrease of the capacity; however, the MoO_2-GO composites can maintain a specific capacity up to of 523.7 mA h g^{-1} after 30 cycles. Compared with pure MoO_2 nanoparticles (Figure S1, Supporting Information), the MoO_2-GO composites possessing the hierarchical structure are generated by the facile hydrothermal method, which could accommodate the volume expansion of the composites effectively during the charging/discharging process, contributing to stabilizing the robust nanostructure and thus retaining good cycling stability. When cycled at a current density of 500 mA g^{-1}, a discharge capacity of 506.6 mA h g^{-1} could be obtained in the first cycle. With the increasing cycles, the capacity is retained at 310.4 mA h g^{-1}. The capacity values are higher than those of the MoO_2 nanoparticles (Figure S1, Supporting Information), indicating that the GO support within MoO_2 nanoparticles benefits the improvement of the electrochemical properties of the MoO_2 anode. The cycling stability of the MoO_2-GO composites over the MoO_2 nanoparticles could be mainly ascribed to the interconnection of the carbon network that encapsulates the nanoparticles to form a stable structure on the GO in order to restrain volume change, leading to the a good cycling performance. The reduced capacity probably results from the aggregation of the pulverized particles during the insertion/extraction process,[24,47,48] which needs to be further investigated.

In order to figure out why the MoO_2-GO composites have enhanced electrochemical performance compared to the MoO_2

dx.doi.org/10.1021/jp508933c | J. Phys. Chem. C 2014, 118, 24890−24897

nanoparticles, Nyquist plots of the AC impedance analysis were measured in Figure 5d. It is obvious that the impedance spectra were composed of three parts: R_f could be assigned to the electrolyte resistance in the high frequency semicircle. The electrode reaction of the electrode−electrolyte interface can be represented by the charge transfer resistance R_{ct} in the low frequency semicircle.[49−51] A straight line on the low frequency end of the electrode arc intersecting the real impedance stands for the Warburg impedance.[51,52] From the Nyquist plots, it gives better separation between charge transfer and diffusion process. The semicircle for the MoO_2-GO composite electrode in the high frequency region is much smaller than that of the MoO_2 nanoparticle electrode; these results suggest that the MoO_2-GO composites electrode has a much lower charge transfer resistance (44Ω) than that of the MoO_2 nanoparticles electrodes (with the charge transfer resistance more than 300Ω). The slope of the linear dependence of the MoO_2-GO composites electrode in the low frequency region is much bigger than that of the MoO_2 nanoparticles electrode, indicating that it has a higher diffusion coefficient of lithium-ions. These values confirm that MoO_2-GO composites have a more conductive pathway for lithium-ions transportation than the pure MoO_2 nanoparticles. The above results claimed that the incorporative effect in GO and MoO_2 not only improve the conductivity of the nanocomposites, but enable charge transfer kinetics in the composites, which greatly ease the development of the electrochemical reaction between the electrolyte and active materials, resulting in enhancement in the electrochemical properties.

According to the above results, the cycling stability and discharge capacity of the MoO_2-GO composites is improved compared with those of the pure MoO_2 nanoparticles, which may be attributed to the novel nanoarchitecture consisting of carbon network of GO. First, the small dimensional MoO_2 nanoparticles can offer a shortened transport length for lithium-ion diffusion, which leads to the kinetically feasible conversion reaction. Second, the MoO_2-GO composites with an enlarged surface area and low charge transfer resistance can allow sufficient infiltration of electrolyte and provide more active sites for lithium-ion intercalation/deintercalation. Third, GO can not only act as an effective conductive network, but also alleviate volume change during Li-ions intercalation/de-intercalation in the charging/discharging process. Finally, the synergetic effects of MoO_2 and GO could contribute to the robust skeleton, which benefits cycling stability. As a result, the enhanced electrochemical performance of the MoO_2-GO composites could be attributed to its small nanocrystallites, large specific surface area, interrelated conductive carbon network, and incorporation of the novel nanostructure.

4. CONCLUSIONS

In summary, MoO_2-GO composites were synthesized via a facile and environmentally friendly hydrothermal method for the first time. The sizes of MoO_2 nanoparticles in MoO_2-GO composites were tailored to as small as 5−15 nm, which were randomly loaded on the interconnected and conductive GO nanosheets. It was found that the three-dimensional nanoarchitecture could not only afford a highly conductive network for lithium-ion intercalation but also suppress the growth and agglomeration of MoO_2 during the charging/discharging process. The MoO_2-GO composites exhibited an improved storage capacity and cycling performance when compared to the pure MoO_2 nanoparticles. The improved electrochemical performance can be attributed to their unique structure and the support of GO, which can facilitate lithium-ion diffusion and serve as a rapid pathway for lithium-ions and electrons to transport more rapidly. The EIS results also confirmed that the graphene nanosheets provide a superior flexible and conductive framework and greatly enhance the electron rapid transfer of the MoO_2-GO composites during the electrochemical reaction. Therefore, the results indicated that this facile and green strategy can also be used for other metal oxides supported on GO sheets to improve their electrochemical performances. The enhanced capacity and cycling performance make the MoO_2-GO composites a promising anode material for LIBs.

■ ASSOCIATED CONTENT

Supporting Information

Figure S1 giving the cycling performance of the pure MoO_2 nanoparticles. This material is available free of charge via the Internet at http://pubs.acs.org.

■ AUTHOR INFORMATION

Corresponding Authors

*E-mail: chenw@whut.edu.cn. Tel.: +86-27-87651107. Fax: +86-27-87760129.

*E-mail: gzcao@u.washington.edu. Tel.: +1-206-616-9084. Fax: +1-206-543-3100.

Notes

The authors declare no competing financial interest.

■ ACKNOWLEDGMENTS

This work was supported by the International Science & Technology Cooperation Program of China (2013DFR50710), and National Natural Science Foundation of China (51202174). Shan Hu would also appreciate a scholarship for Ph.D. study of the China Scholarship Council (CSC) at the University of Washington.

■ REFERENCES

(1) Xia, X.; Tu, J.; Zhang, Y.; Chen, J.; Wang, X.; Gu, C.; Guan, C.; Luo, J.; Fan, H. J. Porous Hydroxide Nanosheets on Preformed Nanowires by Electrodeposition: Branched Nanoarrays for Electrochemical Energy Storage. *Chem. Mater.* **2012**, *24*, 3793−3799.

(2) Tobishima, S. I.; Takei, K.; Sakurai, Y.; Yamaki, J. I. Lithium Ion Cell Safety. *J. Power Sources* **2000**, *90*, 188−195.

(3) Recham, N.; Chotard, J. N.; Dupont, L.; Delacourt, C.; Walker, W.; Armand, M.; Tarascon, J.-M. A 3.6 V Lithium-Based Fluorosulphate Insertion Positive Electrode for Lithium-Ion Batteries. *Nat. Mater.* **2009**, *9*, 68−74.

(4) Kang, B.; Ceder, G. Battery Materials for Ultrafast Charging and Discharging. *Nature* **2009**, *458*, 190−193.

(5) Goodenough, J. B.; Kim, Y. Challenges for Rechargeable Li Batteries. *Chem. Mater.* **2009**, *22*, 587−603.

(6) Li, H.; Wang, Z.; Chen, L.; Huang, X. Research on Advanced Materials for Li-Ion Batteries. *Adv. Mater.* **2009**, *21*, 4593−4607.

(7) Padhi, A. K.; Nanjundaswamy, K.; Goodenough, J. B. D. Phospho-Olivines as Positive-Electrode Materials for Rechargeable Lithium Batteries. *J. Electrochem. Soc.* **1997**, *144*, 1188−1194.

(8) Dunn, B.; Kamath, H.; Tarascon, J. M. Electrical Energy Storage for the Grid: A Battery of Choices. *Science* **2011**, *334*, 928−935.

(9) Tarascon, J. M.; Armand, M. Issues and Challenges Facing Rechargeable Lithium Batteries. *Nature* **2001**, *414*, 359−367.

(10) Poizot, P.; Dolhem, F. Clean Energy New Deal for a Sustainable World: From Non-Co_2 Generating Energy Sources to Greener Electrochemical Storage Devices. *Energy Environ. Sci.* **2011**, *4*, 2003−2019.

(11) Bruce, P. G.; Scrosati, B.; Tarascon, J. M. Nanomaterials for Rechargeable Lithium Batteries. *Angew. Chem., Int. Ed.* **2008**, *47*, 2930−2946.
(12) Jiang, C.; Hosono, E.; Zhou, H. Nanomaterials for Lithium Ion Batteries. *Nano Today* **2006**, *1*, 28−33.
(13) Aricò, A. S.; Bruce, P.; Scrosati, B.; Tarascon, J. M.; Van Schalkwijk, W. Nanostructured Materials for Advanced Energy Conversion and Storage Devices. *Nat. Mater.* **2005**, *4*, 366−377.
(14) Shi, Y.; Guo, B.; Corr, S. A.; Shi, Q.; Hu, Y. S.; Heier, K. R.; Chen, L.; Seshadri, R.; Stucky, G. D. Ordered Mesoporous Metallic MoO_2 Materials with Highly Reversible Lithium Storage Capacity. *Nano Lett.* **2009**, *9*, 4215−4220.
(15) Liu, B.; Zhao, X.; Tian, Y.; Zhao, D.; Hu, C.; Cao, M. A Simple Reduction Process to Synthesize MoO_2/C Composites with Cage-Like Structure for High-Performance Lithium-Ion Batteries. *Phys. Chem. Chem. Phys.* **2013**, *15*, 8831−8837.
(16) Chen, Y.; Di, X.; Ma, C.; Zhu, C.; Gao, P.; Li, J.; Sun, C.; Ouyang, Q. Graphene-MoO_2 Hierarchical Nanoarchitectures: In Situ Reduction Synthesis and High Rate Cycling Performance as Lithium-Ion Battery Anodes. *RSC Adv.* **2013**, *3*, 17659−17663.
(17) Wyckoff, R. W. G.; Wyckoff, R. *Crystal Structures*; Interscience publishers: New York, 1963; Vol. *1*.
(18) Dahn, J.; McKinnon, W. Structure and Electrochemistry of Li_XMoO_2. *Solid State Ionics* **1987**, *23*, 1−7.
(19) Brandt, B. G.; Skapski, A. A Refinement of Crystal Structure of Molybdenum Dioxide. *Acta Chem. Scand.* **1967**, *21*.
(20) Auborn, J.; Barberio, Y.; Hanson, K.; Schleich, D.; Martin, M. Amorphous Molybdenum Sulfide Electrodes for Nonaqueous Electrochemical Cells. *J. Electrochem. Soc.* **1987**, *134*, 580−586.
(21) Murphy, D.; Di Salvo, F.; Carides, J.; Waszczak, J. Topochemical Reactions of Rutile Related Structures with Lithium. *Mater. Res. Bull.* **1978**, *13*, 1395−1402.
(22) Ku, J. H.; Jung, Y. S.; Lee, K. T.; Kim, C. H.; Oh, S. M. Thermoelectrochemically Activated MoO_2 Powder Electrode for Lithium Secondary Batteries. *J. Electrochem. Soc.* **2009**, *156*, A688−A693.
(23) Zeng, L.; Zheng, C.; Deng, C.; Ding, X.; Wei, M. MoO_2-Ordered Mesoporous Carbon Nanocomposite as an Anode Material for Lithium-Ion Batteries. *ACS Appl. Mater. Interfaces* **2013**, *5*, 2182−2187.
(24) Liu, Y.; Zhang, H.; Ouyang, P.; Li, Z. One-Pot Hydrothermal Synthesized MoO_2 with High Reversible Capacity for Anode Application in Lithium Ion Battery. *Electrochim. Acta* **2013**, *102*, 429−435.
(25) Zhang, H. J.; Wu, T. H.; Wang, K. X.; Wu, X. Y.; Chen, X. T.; Jiang, Y. M.; Wei, X.; Chen, J. S. Uniform Hierarchical MoO_2/Carbon Spheres with High Cycling Performance for Lithium Ion Batteries. *J. Mater. Chem. A* **2013**, *1*, 12038−12043.
(26) Sun, Y.; Hu, X.; Luo, W.; Huang, Y. Self-Assembled Hierarchical MoO_2/Graphene Nanoarchitectures and Their Application as a High-Performance Anode Material for Lithium-Ion Batteries. *ACS Nano* **2011**, *5*, 7100−7107.
(27) Yang, L.; Liu, L.; Zhu, Y.; Wang, X.; Wu, Y. Preparation of Carbon Coated MoO_2 Nanobelts and Their High Performance as Anode Materials for Lithium Ion Batteries. *J. Mater. Chem.* **2012**, *22*, 13148−13152.
(28) Wang, Z.; Chen, J. S.; Zhu, T.; Madhavi, S.; Lou, X. W. One-Pot Synthesis of Uniform Carbon-Coated MoO_2 Nanospheres for High-Rate Reversible Lithium Storage. *Chem. Commun.* **2010**, *46*, 6906−6908.
(29) Xu, Y.; Yi, R.; Yuan, B.; Wu, X.; Dunwell, M.; Lin, Q.; Fei, L.; Deng, S.; Andersen, P.; Wang, D. High Capacity MoO_2/Graphite Oxide Composite Anode for Lithium-Ion Batteries. *J. Phys. Chem. Lett.* **2012**, *3*, 309−314.
(30) Yoo, E. J.; Kim, J.; Hosono, E.; Zhou, H.; Kudo, T.; Honma, I. Large Reversible Li Storage of Graphene Nanosheet Families for Use in Rechargeable Lithium Ion Batteries. *Nano Lett.* **2008**, *8*, 2277−2282.
(31) Wang, G.; Shen, X.; Yao, J.; Park, J. Graphene Nanosheets for Enhanced Lithium Storage in Lithium Ion Batteries. *Carbon* **2009**, *47*, 2049−2053.
(32) Landi, B. J.; Ganter, M. J.; Cress, C. D.; DiLeo, R. A.; Raffaelle, R. P. Carbon Nanotubes for Lithium Ion Batteries. *Energy Environ. Sci.* **2009**, *2*, 638−654.
(33) Zhao, X.; Cao, M.; Liu, B.; Tian, Y.; Hu, C. Interconnected Core−Shell MoO_2 Microcapsules with Nanorod-Assembled Shells as High-Performance Lithium-Ion Battery Anodes. *J. Mater. Chem.* **2012**, *22*, 13334−13340.
(34) Seng, K. H.; Du, G. D.; Li, L.; Chen, Z. X.; Liu, H. K.; Guo, Z. P. Facile Synthesis of Graphene−Molybdenum Dioxide and Its Lithium Storage Properties. *J. Mater. Chem.* **2012**, *22*, 16072−16077.
(35) Tang, Q.; Shan, Z.; Wang, L.; Qin, X. MoO_2-Graphene Nanocomposite as Anode Material for Lithium-Ion Batteries. *Electrochim. Acta* **2012**, *79*, 148−153.
(36) Hummers, W. S., Jr.; Offeman, R. E. Preparation of Graphitic Oxide. *J. Am. Chem. Soc.* **1958**, *80*, 1339−1339.
(37) Cao, G.; Zhang, M.; Yan, F.; Tang, X.; Li, Q.; Wang, T. Flexible CoO-Graphene-Carbon Nanofiber Mats as Binder-Free Anodes for Lithium-Ion Batteries with Superior Rate Capacity and Cyclic Stability. *J. Mater. Chem. A* **2014**, *2*, 5890−5897.
(38) Uchaker, E.; Zhou, N.; Li, Y.; Cao, G. Polyol-Mediated Solvothermal Synthesis and Electrochemical Performance of Nanostructured V_2O_5 Hollow Microspheres. *J. Phys. Chem. C* **2013**, *117*, 1621−1626.
(39) Han, P.; Ma, W.; Pang, S.; Kong, Q.; Yao, J.; Bi, C.; Cui, G. Graphene Decorated with Molybdenum Dioxide Nanoparticles for Use in High Energy Lithium Ion Capacitors with an Organic Electrolyte. *J. Mater. Chem. A* **2013**, *1*, 5949−5954.
(40) Zhou, L.; Wu, H. B.; Wang, Z.; Lou, X. W. Interconnected MoO_2 Nanocrystals with Carbon Nanocoating as High-Capacity Anode Materials for Lithium-Ion Batteries. *ACS Appl. Mater. Interfaces* **2011**, *3*, 4853−4857.
(41) Dahn, J. R.; McKinnon, W. R. Structure and Electrochemistry of Li_xMoO_2. *Solid State Ionics* **1987**, *23*, 1−7.
(42) Kang, Y. M.; Kim, K. T.; Lee, K. Y.; Lee, S.-J.; Jung, J. H.; Lee, J. Y. Improvement of Initial Coulombic Efficiency of Co_3O_4 by Ballmilling Using Ni as an Additive. *J. Electrochem. Soc.* **2003**, *150*, A1538−A1543.
(43) Zhang, H. J.; Wang, K. X.; Wu, X. Y.; Jiang, Y. M.; Zhai, Y. B.; Wang, C.; Wei, X.; Chen, J. S. MoO_2/Mo_2C Heteronanotubes Function as High-Performance Li-Ion Battery Electrode. *Adv. Funct. Mater.* **2014**, *22*, 3399−3404.
(44) Zhang, X.; Song, X.; Gao, S.; Xu, Y.; Cheng, X.; Zhao, H.; Huo, L. Facile Synthesis of Yolk-Shell MoO_2 Microspheres with Excellent Electrochemical Performance as a Li-Ion Battery Anode. *J. Mater. Chem. A* **2013**, *1*, 6858−6864.
(45) Zhang, M.; Li, Y.; Uchaker, E.; Candelaria, S.; Shen, L.; Wang, T.; Cao, G. Homogenous Incorporation of SnO_2 Nanoparticles in Carbon Cryogels Via the Thermal Decomposition of Stannous Sulfate and Their Enhanced Lithium-Ion Intercalation Properties. *Nano Energy* **2013**, *2*, 769−778.
(46) Hong, Z.; Wei, M.; Lan, T.; Jiang, L.; Cao, G. Additive-Free Synthesis of Unique TiO_2 Mesocrystals with Enhanced Lithium-Ion Intercalation Properties. *Energy Environ. Sci.* **2012**, *5*, 5408−5413.
(47) Pereira-Ramos, J. P.; Kumagai, N.; Kumagai, N. Low Temperature Molybdenum Oxide as Host Lattice for Lithium Intercalation. *J. Power Sources* **1995**, *56*, 87−90.
(48) Jung, Y. S.; Lee, S.; Ahn, D.; Dillon, A. C.; Lee, S. H. Electrochemical Reactivity of Ball-Milled MoO_3 as Anode Materials for Lithium-Ion Batteries. *J. Power Sources* **2009**, *188*, 286−291.
(49) Umeda, M.; Dokko, K.; Fujita, Y.; Mohamedi, M.; Uchida, I.; Selman, J. Electrochemical Impedance Study of Li-Ion Insertion into Mesocarbon Microbead Single Particle Electrode: Part I. Graphitized Carbon. *Electrochim. Acta* **2001**, *47*, 885−890.
(50) Chang, Y.-C.; Sohn, H.-J. Electrochemical Impedance Analysis for Lithium Ion Intercalation into Graphitized Carbons. *J. Electrochem. Soc.* **2000**, *147*, 50−58.

(51) Zhang, S.; Xu, K.; Jow, T. Electrochemical Impedance Study on the Low Temperature of Li-Ion Batteries. *Electrochim. Acta* **2004**, *49*, 1057−1061.
(52) Orazem, M. E.; Tribollet, B. *Electrochemical Impedance Spectroscopy*; Wiley-Interscience, 2011; Vol. *48*.